Received: 3 October 2023 | Revised: 8 March 2024 | Accepted: 16 March 2024

IET Renewable Power Generation

DOI: 10.1049/rpg2.13111

The Institution of Engineering and Technology WILEY

ORIGINAL RESEARCH

Design optimization of inner and outer-rotor PMSGs for X-ROTOR wind turbines

Reza Yazdanpanah[1] | **Seyed Abolfazl Mortazavizadeh**[1] | **Mohammad Salehian**[2] | **David Campos-Gaona**[1] | **Olimpo Anaya-Lara**[1]

[1]Wind Energy and Control Centre, Electronic and Electrical Engineering, University of Strathclyde, Glasgow, UK

[2]Digital Medicines Manufacturing Research Centre, University of Strathclyde, Glasgow, UK

Correspondence
Reza Yazdanpanah, Wind Energy & Control Centre, Department of Electronic and Electrical Engineering, University of Strathclyde, Royal College Building, 204 George Street, Glasgow G1 1XW, UK.
Email: reza.yazdanpanah@strath.ac.uk

Funding information
European Union's Horizon 2020 Research and Innovation Programme, Grant/Award Number: 101007135; Horizon 2020 Framework Programme, Grant/Award Number: 101007135

Abstract

This article presents an analytical design approach for the inner and outer rotor Permanent Magnet Synchronous Generators (PMSGs) that are a key component of wind turbines. By developing the analytical model, sensitivity analysis has been performed to determine the effect of some important geometrical and electromagnetic parameters on the generator's output characteristics. The GA optimization algorithm was used to find optimized designs in terms of efficiency, weight, cost, and temperature rise. In order to find the global optimization solution within the allowed variable range and in accordance with the constraints, a combined objective function has also been defined. In order to validate the analytical model, ANSYS electromagnetic and thermal simulations have been used. With this approach, the designer is provided with a good understanding of the input parameters and constraints in light of the application requirements.

1 | INTRODUCTION

As a first step towards an affordable, reliable, clean power system that meets zero net carbon emissions, the United States will need to double solar and wind deployments through the 2020s (60 GW/year) and nearly triple historical maximums by 2030 (80 GW/year) before achieving the promise of zero net carbon emissions [1]. The European Union (EU) has set an ambitious target of introducing 300 GW of offshore wind power in the region to move toward cleaner energy networks [2]. In the future Norwegian energy mix, offshore wind appears to be the dominant source of power due to opposition to onshore wind power development and limited potential for hydropower and solar power expansion [3]. Many advantages are associated with offshore wind farms, such as higher full-load hours per year, longer lifetimes, reduced visual impacts, lower noise, and up to 20% higher rotor speeds [4–6].

The X-shaped Radical Offshore Wind Turbine for Overall Cost of Energy Reduction (X-ROTOR) project aims to develop a hybrid vertical-horizontal axis wind turbine using an X-shaped rotor [7]. A feasibility study indicates that this concept could reduce the cost of energy by 20–30% by reducing operational and maintenance costs [8]. Moreover, the X-ROTOR concept offers a fresh perspective on vertical axis wind turbines, a design that has yet to be commercially successful on a large scale [9]. For the X-ROTOR structure, a rotation around the vertical axis increases the wind speed of secondary HAWT rotors, which increases energy capture based on rotor size, and provides rotational symmetry so that the turbines do not need to be yawed. In this arrangement, the secondary HAWT rotors have a large increase in speed; this allows a direct-drive system without a multipole generator to be used [7, 8].

The generators of wind power plants are one of the most important factors that need to be addressed to improve the performance and efficiency. A variety of wind power plant configurations, including synchronous generators, have now been introduced and used. Due to recent technological advancements in power converters and permanent magnet materials, direct-drive (DD) PMSGs are attracting more attention from researchers and wind turbine manufacturers. Offshore wind

turbines now use DD-PMSGs more and more because their gearboxes are increasingly complex and massive as they produce more power. In addition to producing higher energy, DD generators are more reliable and last longer. DD generators are, however, very large, which represents a challenge that needs to be addressed [10, 11].

A number of topologies of PMSGs have also been proposed to address the issue of large-sized DD-PSMGs, including outer-rotor surface mounted PMSGs, inner-rotor surface mounted PMSGs, and interior PMSGs [12]. In some research, outer-rotors are used because of their low manufacturing costs and ease of construction. In order to achieve high efficiency and high-power density, it is necessary to consider the cooling systems for outer-rotor structures. However, further efforts need to be made to develop machines that can reduce the weight of DD-PMSGs with high power. Researchers have previously reported difficulties scaling up to several megawatts or more. Especially for offshore applications, the resulting designs are excessively large and/or massive, which pose major logistical challenges [13]. In this article, an optimal design methodology is presented to solve this problem.

For the design procedure of electric machines, a number of optimization algorithms have been developed to find an optimal design. The first algorithms implemented were deterministic and direct research algorithms. In the last few years, gradient-free stochastic algorithms, like particle swarm optimization and genetic algorithms (GAs), have taken over. A review of the GA shows that it is an efficient method for finding an optimal solution for designing electric machines, allowing individuals from generations to be discarded that cannot fit constraints.

This article is organized as follows. In Section 2, the analytical model and the principle of the design methodology are presented, and in Section 3, the results of the analytical model are verified by comparing them to finite element results. A sensitivity analysis of some of the most important design variables is presented in Section 4, as well as an analysis of their effects on the output characteristics. Lastly, Section 5 presents the optimization method, optimized designs, and a comparison with some other studies.

2 | SURFACE MOUNTED PMSG

Two types of generators are commonly used in wind turbines; induction generators and PMSGs. Recently, PMSGs are widely preferred due to their high-power densities. Furthermore, they are low in space occupancy, highly efficient, low in noise, direct drive, and low in vibration.

2.1 | Inner and outer-rotor structures

PMSGs are fabricated as inner and outer rotor forms. Figure 1 shows the structures of inner-rotor and outer-rotor PMSGs. The average radius (r_g) between the stator and the rotor is considered as the air-gap radius and will be used in the analytical design equations.

Considering the simplified linear model, there is no difference between inner and outer topologies in flux paths and the electromagnetic characteristics, but some geometrical, electrical, and thermal parameters will be different.

The following assumptions are taken into account in the design of the PMSG [14]:

- Only the fundamental component of the magnetic flux density distribution in the airgap is considered.
- The magnetic flux density perpendicularly crosses the airgap.

2.2 | Analytical model

In this section, based on the magnetic equivalent circuit and the flux path, the geometrical and electrical parameters are calculated.

The fundamental harmonic of the air-gap flux density due to the magnets is [14]:

$$\widehat{B}_{g1} = \widehat{B}_g \frac{4}{\pi} \sin\left(\frac{\pi}{2}\alpha\right); \quad \widehat{B}_g = \frac{l_m}{\mu_{rm}.g_e} B_{rm}, \tag{1}$$

where B_{rm} is the remnant flux density of the magnets, l_m is the magnet height, α is the PM width to pole pitch ratio, and:

$$g_e = K_c.g_1; \quad g_1 = g + \frac{l_m}{\mu_{rm}}, \tag{2}$$

where g is the airgap length and the Carter factor is defined as:

$$K_c = \frac{\tau_{slot}}{\tau_{slot} - g_1.\gamma}; \quad \gamma = \frac{4}{\pi}\left[\frac{w_s}{2g_1}\tan^{-1}\left(\frac{w_s}{2g_1}\right) - \log\left(\sqrt{1+\left(\frac{w_s}{2g_1}\right)^2}\right)\right], \tag{3}$$

where w_s is the slot opening and τ_{slot} the slot pitch.

The no-load phase voltage induced by this flux density in a stator winding can be calculated as [15]:

$$E_{rms} = \sqrt{2}.K_w.N_{ph}.\omega_m.r_g.L.\widehat{B}_{g1}, \tag{4}$$

where K_w is the winding factor, N_{ph} the phase number of turns, ω_m the angular mechanical speed, r_g the mean airgap radius, and L the axial length.

The winding factor for concentrated winding could be calculated by [16]:

$$K_w = \frac{\sin(\pi/6)}{q_1.\sin\left(\pi/(6q_1)\right)}. \tag{5}$$

The stator electrical loading is defined as:

$$A = \frac{2.m.N_{ph}}{2\pi.r_g} I_{rms}, \tag{6}$$

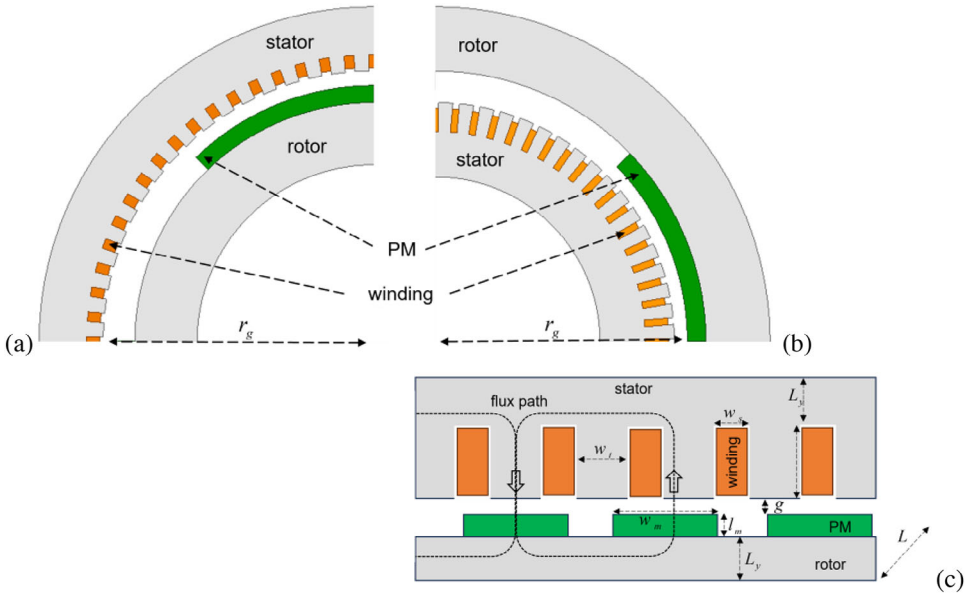

FIGURE 1 The structures of inner-rotor and outer-rotor PMSGs; (a) inner-rotor, (b) outer-rotor and (c) linearized model.

where m is the number of phases, and I_{rms} the phase current.

So, the average apparent power transferred through the air-gap over one period of the power source can be written in terms of the instantaneous induced voltage and the current equations as:

$$S_g = m.E_{rms}.I_{rms} = \sqrt{2}.\pi.r_g^2.K_w.\omega_m.L.A.\hat{B}_{g1}. \tag{7}$$

Moreover, the pole magnetic flux density is calculated as:

$$H_c l_m = \phi \frac{g_e}{\mu_0 w_m L} \rightarrow \phi = \frac{\mu_0 H_c l_m w_m L}{g_e}, \tag{8}$$

where w_m is the PM width. For the slot and tooth sizing, the maximum allowed flux density (B_t) to prevent saturation should be considered. So, the tooth width, yoke thickness, and slot width are calculated as:

$$\begin{aligned} w_t &= \frac{\phi}{B_t q_1 m L} \\ L_y &= \frac{q_1 m w_t}{2} \\ w_s &= \tau_{slot} - w_t;\ \tau_{slot} = \frac{\pi r_g}{q_1 m.p}. \end{aligned} \tag{9}$$

And the slot depth is calculated based on the phase current, current density (J), and slot fill factor (s_f):

$$h_s = \frac{A_s}{w_s};\ A_s = \frac{I_{rms} N_{ph}}{p.q_1.J.s_f}, \tag{10}$$

where p is the number of pole pairs.

Magnetizing and leakage inductances are calculated as [17]:

$$\begin{aligned} L_m &= \mu_0 \frac{2mr_g}{\pi p^2 g_e} L\left(K_w N_{ph}\right)^2 \\ L_l &= \mu_0 \frac{2}{pq_1} N_{ph}^2 L \frac{h_s}{3w_s}. \end{aligned} \tag{11}$$

And:

$$L_s = L_m + L_l. \tag{12}$$

For calculation of the stator resistance, the average length of one turn of the coil is required:

$$l_{av} = 2L + 4\tau_p, \tag{13}$$

where τ_p is the pole pitch. Then, the resistance will be:

$$R_s = \frac{\rho_{cu} N_{ph}^2 l_{av}}{q_1 A_s s_f p}. \tag{14}$$

Core, copper, and PM weights could be calculated as:

$$\begin{aligned} W_{lam} &= \left\{2\pi.r_r.L_y + 2\pi r_s.L_y + (\tau_s - w_s) l_s.q_1.2p.m\right\}.L.\rho_{lam,m} \\ W_{cu} &= \left\{A_s.l_{av}.q_1.m.p\right\}.\rho_{cu,m} \\ W_{PM} &= \left\{2p.l_m.\tau_p.\alpha\right\}.L.\rho_{PM,m} \\ W_{total} &= W_{lam} + W_{cu} + W_{PM}, \end{aligned} \tag{15}$$

where r_s and r_r are the mean stator and rotor yoke radii, respectively, and $\rho_{.,m}$ is the mass density.

TABLE 1 PMSG specifications.

Parameter	Value	Description
P (kW)	2500	Power
V_n (V)	3300	Rated rms voltage
f (Hz)	25	Frequency
n_s (rpm)	372	Rated speed
p	4	Pole pairs
m	3	Phases
PM	VACOdym	Permanent magnet
Core material	M700-65A	Lamination

And after calculation of the costs of materials used, the total cost will be:

$$C_{total} = C_{lam} + C_{PM} + C_{cu}. \tag{16}$$

The winding copper loss is:

$$P_{cu} = 3R_s I_{ph}^2. \tag{17}$$

And the core loss is calculated by the loss density of the core as:

$$P_{fe} = \left\{ 2P_{fe0h}.\frac{f}{50}\left(\frac{B_t}{1.5}\right)^2 + 2P_{fe0e}\left(\frac{f}{50}\right)^2\left(\frac{B_t}{1.5}\right)^2 \right\} \times W_{lam}. \tag{18}$$

So, the efficiency is calculated as:

$$eff = \frac{P - P_{cu} - P_{fe}}{P}. \tag{19}$$

Finally, the stator heat dissipation area is:

$$A_c = 2\pi\left(r_s \pm \frac{l_y}{2}\right)L\ ;\ \begin{cases} + : \text{inner rotor} \\ - : \text{outer rotor} \end{cases}. \tag{20}$$

And the temperature rise is:

$$\Delta T = \frac{\left(P_{cu} + P_{fe}\right)}{A_c.K_h}, \tag{21}$$

where K_h is the thermal convection coefficient.

3 | ANALYTICAL MODEL VALIDATION

To validate the analytical equations of previous section, a PMSG with the specifications and input parameters of Tables 1 and 2 was simulated numerically in a finite element commercial software (Ansys Electronics Desktop). All material characteristics have been imported.

TABLE 2 Base PMSG input parameters.

Parameter	Value	Description
B_{rm}	1.2 T	PM remanence
μ_{rm}	1.1	PM relative permeability
B_t	1.8 T	Tooth flux density
H_c	860000 A/m	Magnetic coercivity
s_f	0.7	Slot filling factor
P_{fe0h}	1.1	Core loss hysteresis coefficent
P_{fe0e}	0.3	Core loss eddy-current coefficent
k_h	60 W/m^2.°C	Thermal convection coefficient
$C_{lam.}$	0.5$/kg	Lamination cost
C_{PM}	95$/kg	PM cost
C_{cu}	5$/kg	Copper cost
α	0.8	PM angle to pole ratio
q_1	5	Slots per phase per pole
B_1	0.8 T	Airgap flux density
J	4e6 A/m^2	Current density
J_1	33e3 A/m	Electric loading
g	15 mm	Airgap length
r_g	500 mm	Airgap mean radius

TABLE 3 Comparison of analytical and numerical results.

Parameter	Analytical	Numerical
core loss	16 kW	14 kW
synchronous inductance	4.2 mH	4.5 mH
efficiency	98.6%	99%
temperature rise	79°C	82°C

As shown in Figure 2, the magnetic flux density and temperature distribution in the core. As expected, the maximum flux density is about 1.8 T as defined in the initial parameters.

As shown in Figure 3a, the airgap flux density is about 0.78 T, and the no-load induced voltage is about 3% less than the desired value so, both are in good accordance with the analytical results. The small differences in the results are due to 3D effects that have not been included in the 2D analytical model.

The loading characteristics of currents and electrical and mechanical powers are shown in Figure 3b. Regarding the simulation, the analytical and numerical results are compared in Table 3 where it can be seen that the analytical model is verified.

Based on this model validation, the analytical model will be used in the next sections for the sensitivity analysis and design optimization as this model facilitates the optimization algorithm by reducing the time and memory required.

4 | SENSITIVITY ANALYSIS

To study the effect of input parameters on the performance of the PMSG, the last 7 parameters of Table 2 have been

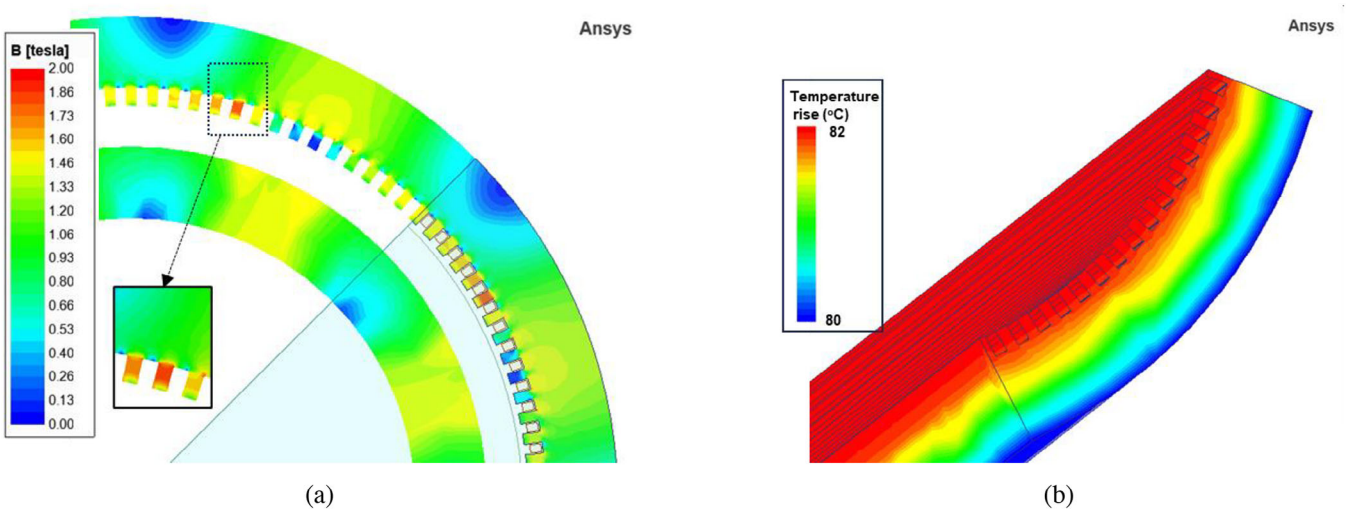

FIGURE 2 Loading simulation results; (a) magnetic flux density in the core and (b) temperature rise in stator.

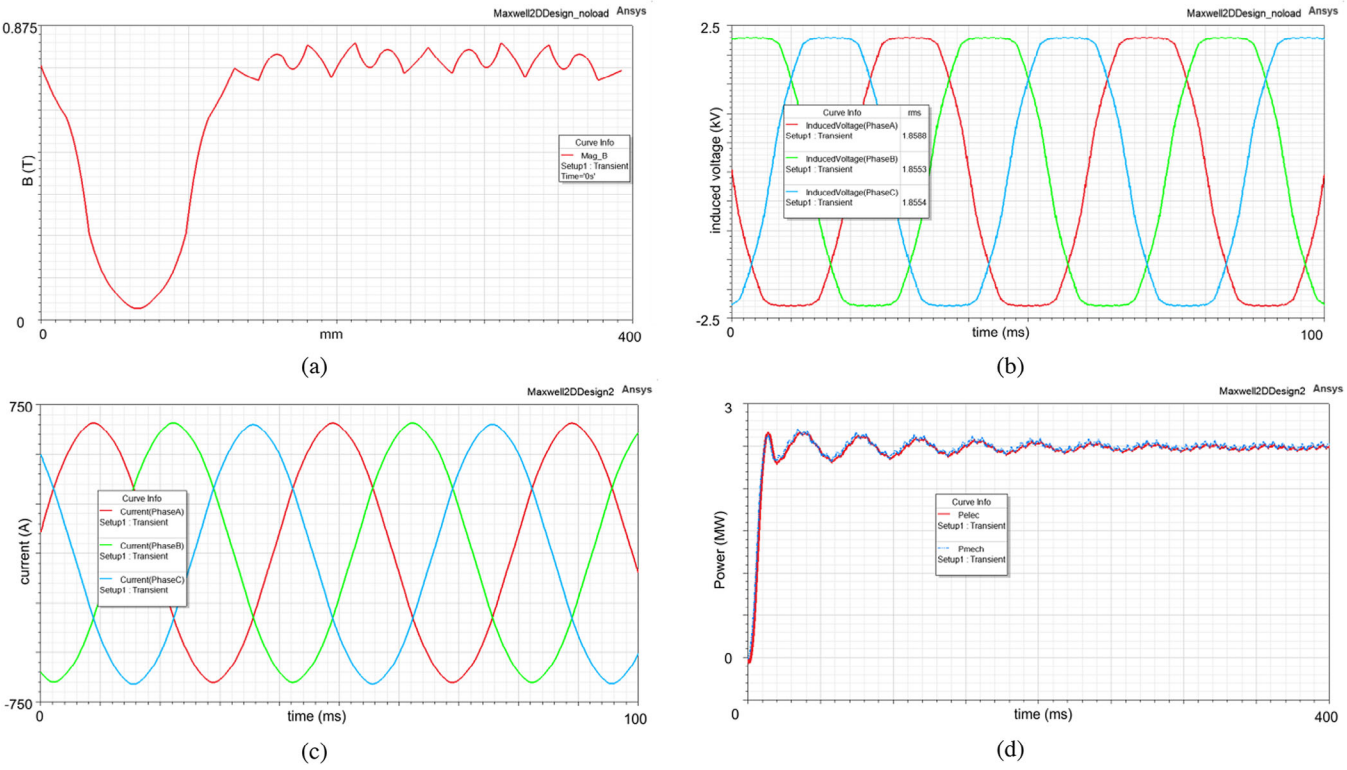

FIGURE 3 Simulation results; (a) no-load airgap flux density, (b) no-load induced voltage, (c) loading current and (d) loading powers.

considered as sweep parameters for sensitivity analysis while the 4 output characteristics are: total weight, total cost, efficiency, and the temperature rise.

Sensitivity analysis examines the effects of a single parameter on the model output while holding the others constant. In this section, we analyze how input parameters and design parameters have affected output performance. On the basis of these analyses, designers can select a reasonable range for optimization parameters. Due to the fact that the output depends on each of the optimization parameters, selecting them individually from the sensitivity analysis is not a sensible decision.

Figure 4 shows the effect of airgap flux density where it has a direct effect on 3 characteristics, but the temperature rise has a maximum at 1T magnetic flux density.

As shown in Figure 5, the electric loading decreases the cost and weight but increases the temperature considerably. This

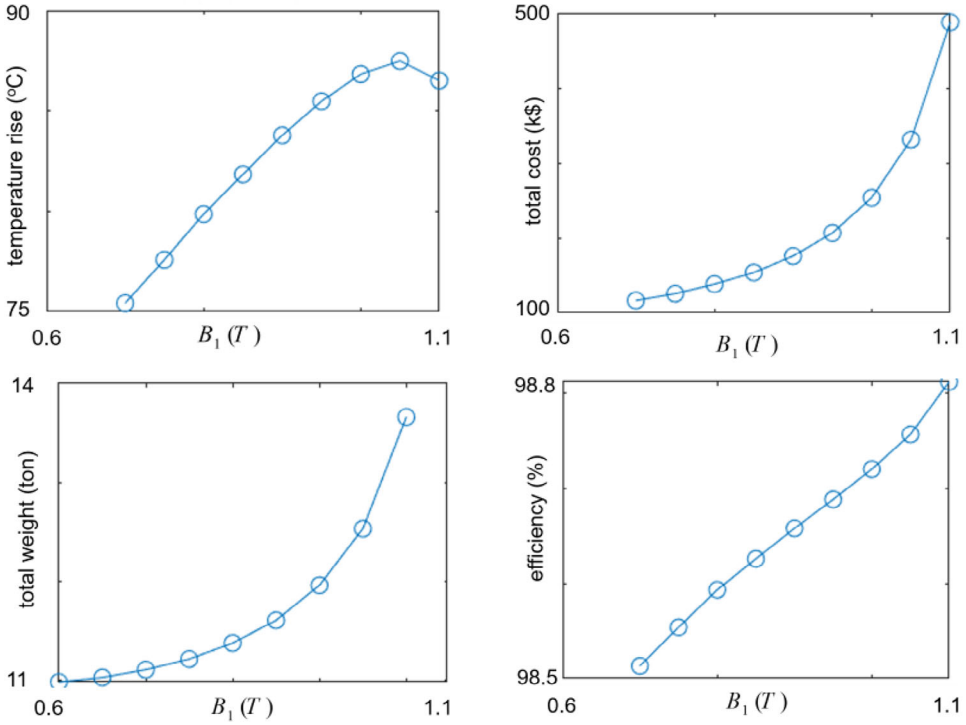

FIGURE 4 The effect of airgap flux density.

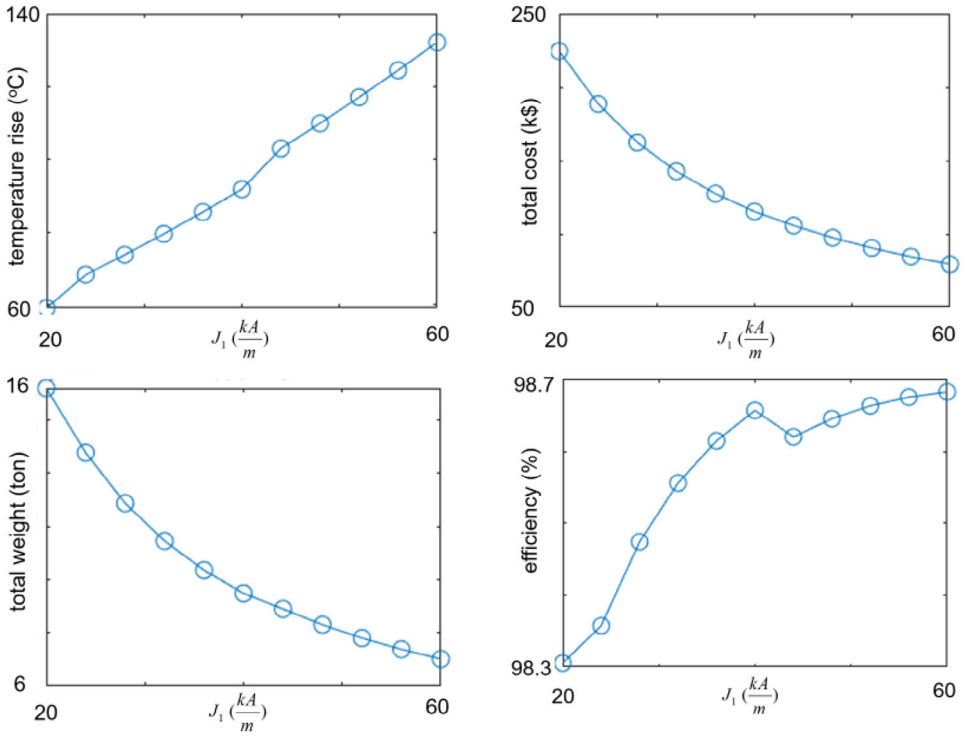

FIGURE 5 The effect of electric loading.

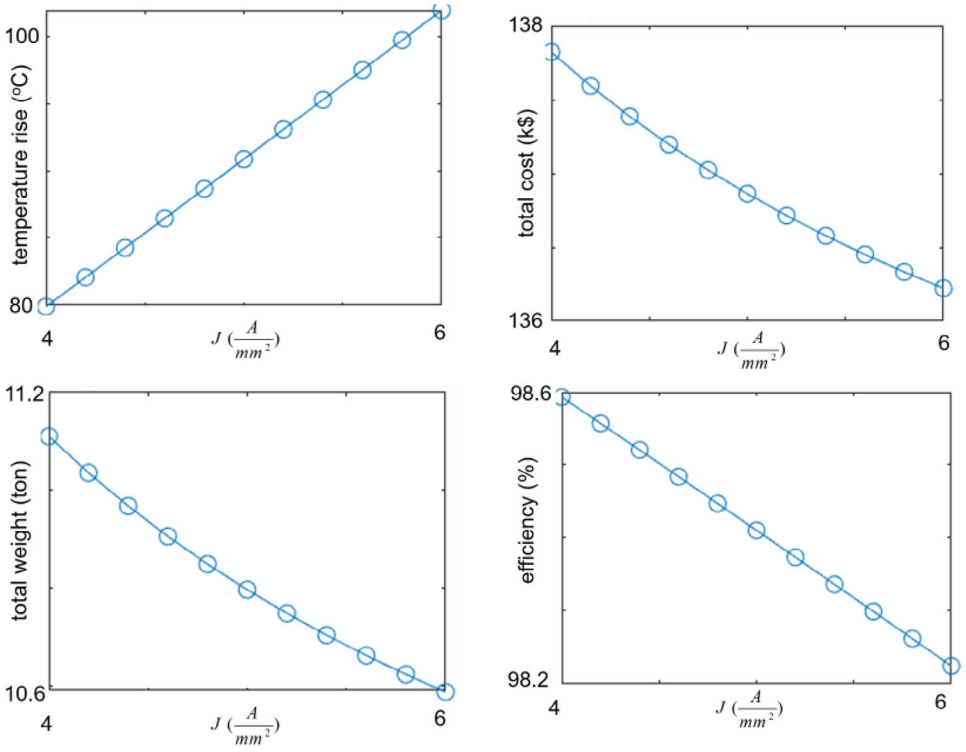

FIGURE 6 The effect of current density.

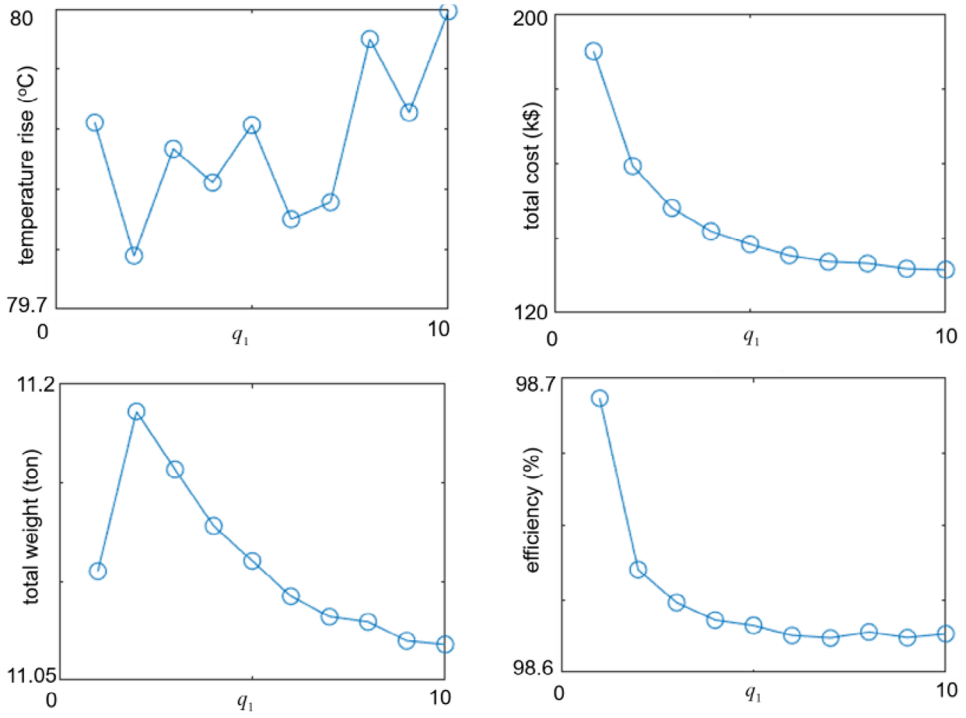

FIGURE 7 The effect of slots per phase per pole.

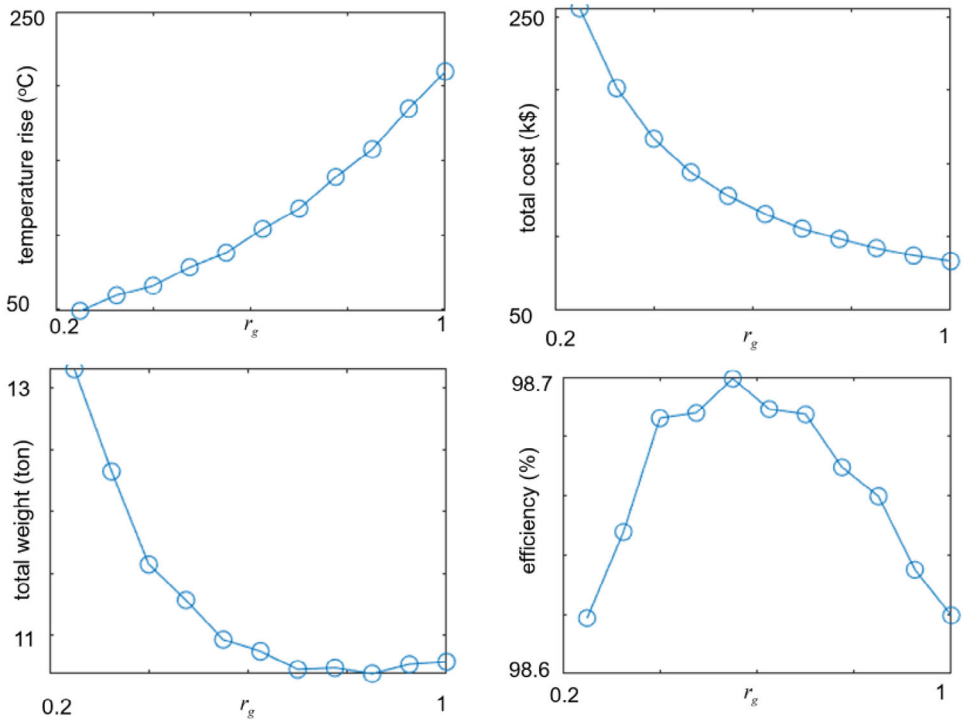

FIGURE 8 The effect of airgap mean radius.

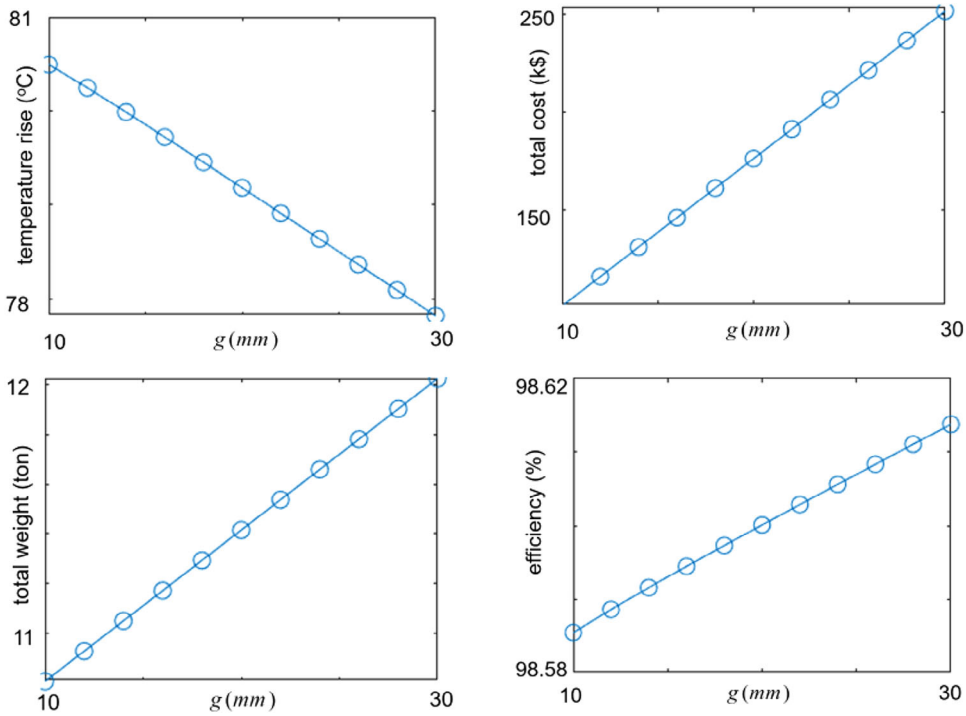

FIGURE 9 The effect of airgap length.

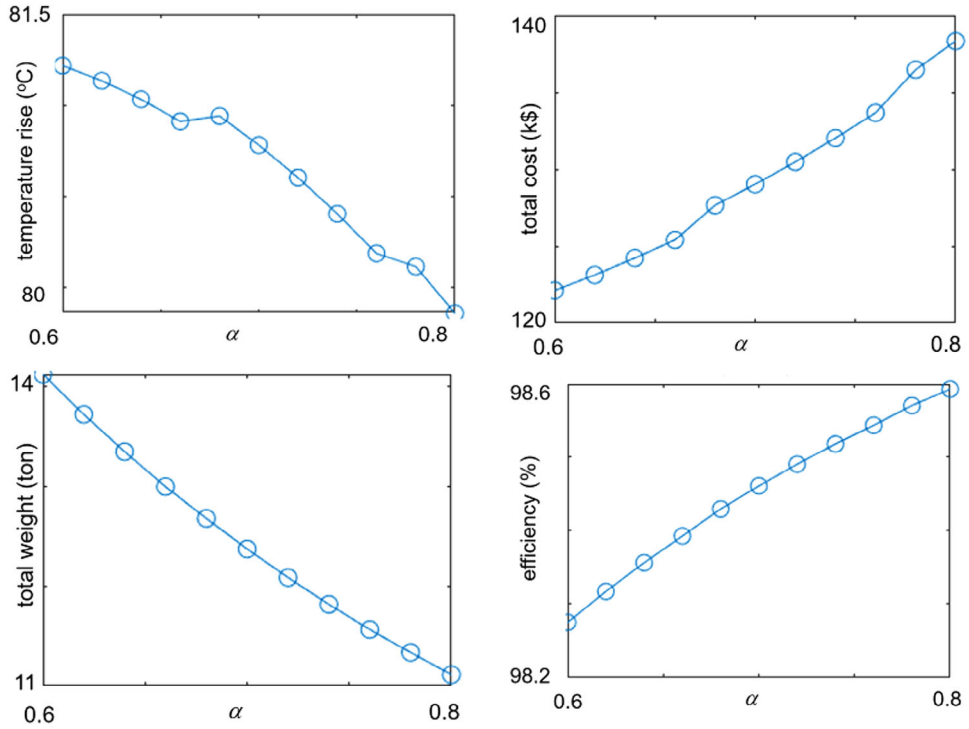

FIGURE 10 The effect of PM to pole pitch ratio.

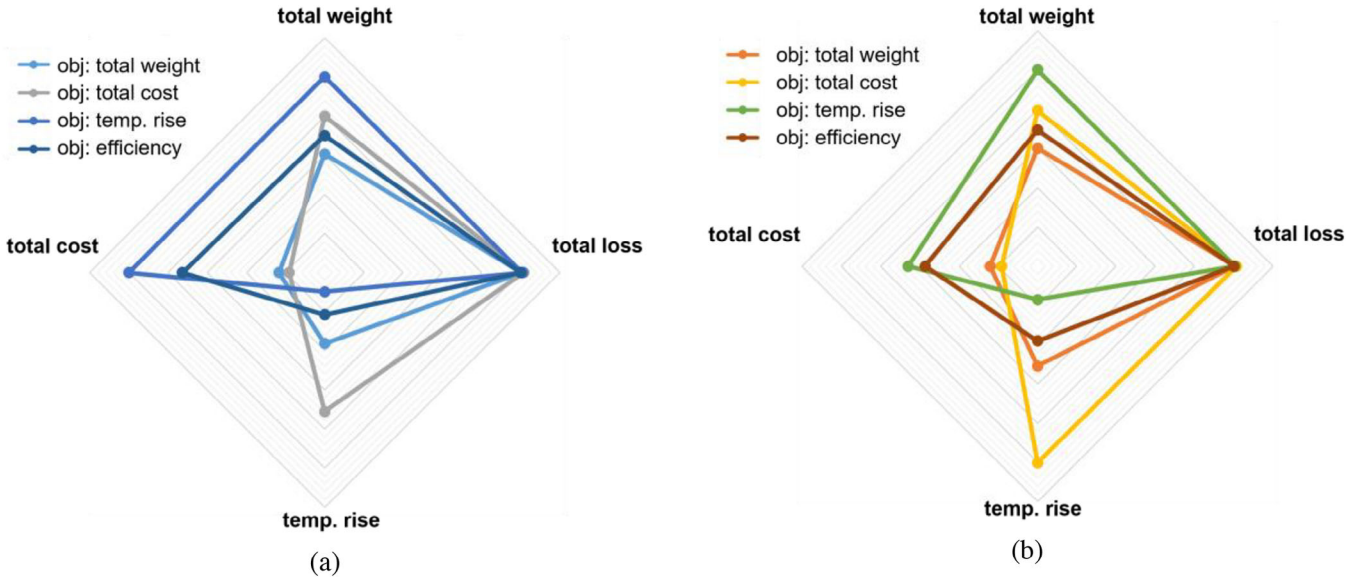

FIGURE 11 Comparison of optimized designs (for first 4 objective functions) in terms of output characteristics. (a) Inner rotor PMSG; (b) outer rotor PMSG.

trend is similar for the current density, except for the efficiency as shown in Figure 6.

As shown in Figure 7, the slot number has negligible effect on the temperature and weight but affects the cost and efficiency greatly. So, it is preferable to use a high slot number if the mechanical constraints allow.

The airgap radius greatly affects the cost, weight, and temperature but has little effect on the efficiency as shown in Figure 8. Nevertheless, as this parameter determines the outer diameter of the machine, it is usually constrained by the application needs.

Similarly, a smaller airgap length is preferable as can be seen in Figure 9, but it is also limited by manufacturing problems.

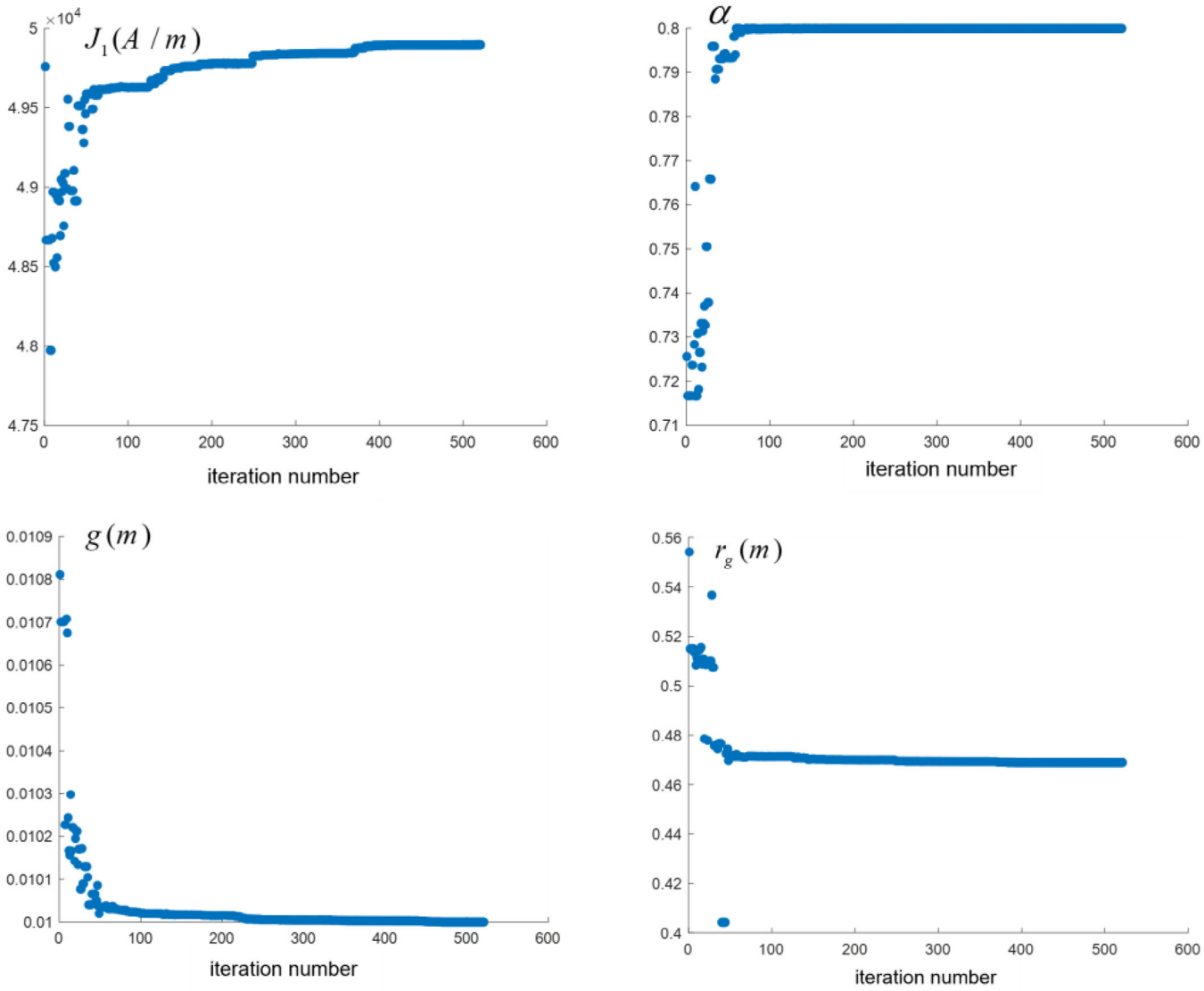

FIGURE 12 Optimization variables over the iterations.

Finally, the PM to pole pitch ratio mostly affects the weight and has no considerable effect on other characteristics as shown in Figure 10.

5 | OPTIMIZATION

5.1 | Optimization algorithm

The model-based optimization was performed using the Genetic Algorithm (GA) to maximize the efficiency and minimize the weight, cost, and temperature rise subject to the constraints. The algorithm was configured to terminate if the discrepancy between the objective value in successive iterations drops below $1e-2$ or if the algorithm completes 300 iterations, whichever condition is met first. The GA was chosen due to its efficiency in searching for the global optimum, handling both continuous and discrete variables, and managing to optimize multiple competing objectives in a multi-objective problem [18]. The computational performance of evolutionary algorithms such as GA can degrade in larger-scale problems with many decision parameters or time-consuming models to calculate the objective function. This can be addressed by using local search methods such as approximate gradient-based algorithms [19] to achieve the optimum point with the minimum number of iterations. More information about the comparison of optimization algorithms can be found in [20].

5.2 | Design optimization

For the GA, the optimization variables and their ranges are selected as shown in Minimizing objective function 5 would

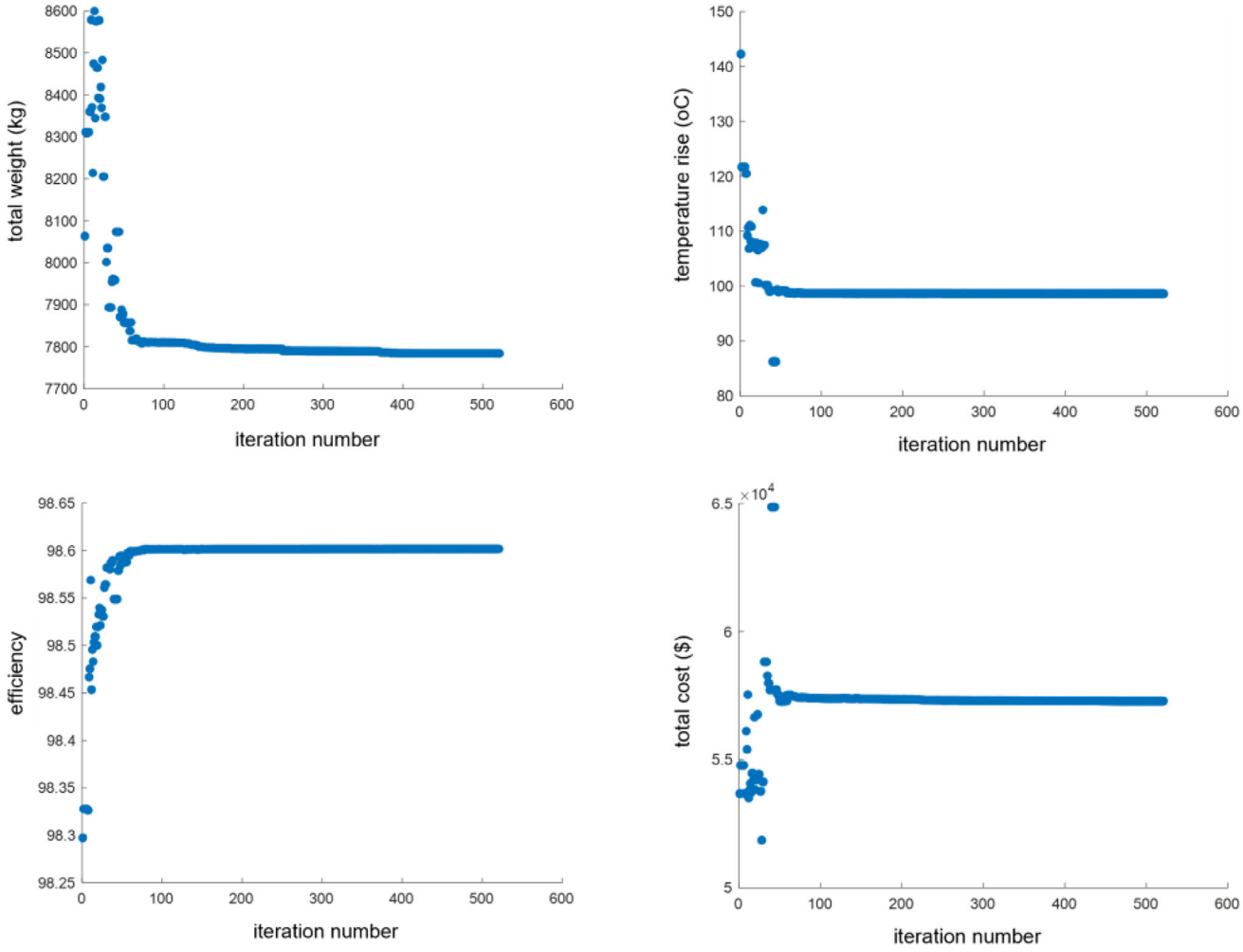

FIGURE 13 Output characteristics over the iterations.

produce the best compromise between cost, temperature, weight, and efficiency. Based on this objective function, the optimal solution may not be equal to the optimal solution based on the other four objective functions, but it may be very close. Each term of objective function 5 can also be given a weighting factor to emphasize some more than others. The optimization constraints are reported in Table 5. These constraints are selected for our application and could be modified as required (Table 4).

To compare the optimization results, different objective functions have been defined as follows:

- **Obj1: Minimize [**total weight**]**
- **Obj2: Minimize [**total cost**]**
- **Obj3: Minimize [**temperature rise**]**
- **Obj4: Maximize [**efficiency**]**
- **Obj5: Minimize [**total weight × total cost × temperature rise ÷ efficiency**]**

The first 4 objective functions investigate a single characteristic and the last one combines 4 output characteristics to find the compromised solution as these characteristics are conflicted. As a result of the importance of cost-effectiveness, we have defined an objective function called "total cost" in our optimization method. By using this objective function, we can design an economically advantageous wind turbine generator.

Minimizing objective function 5 would produce the best compromise between cost, temperature, weight, and efficiency.

TABLE 4 Optimization variables.

Parameter	Min value	Max value	Type
α	0.6	0.8	Continuous
q_1	5	10	Discrete
B_1	0.7 T	0.9 T	Continuous
J	4e6 A/m^2	5e6 A/m^2	Continuous
J_1	30e3 A/m	50e3 A/m	Continuous
g	10 mm	20 mm	Continuous
r_g	200 mm	1000 mm	Continuous

TABLE 5 Optimization constraints.

Characteristic	Constraint
$eff.$	>94%
C_{tot}	<200 k$
W_{tot}	<12 ton
ΔT	<500°C

Based on this objective function, the optimal solution may not be equal to the optimal solution based on the other four objective functions, but it may be very close. Each term of objective function 5 can also be given a weighting factor to emphasize some more than others. The optimization constraints are reported in Table 5. These constraints are selected for our application and could be modified as required.

Figure 11 shows the optimized designs' characteristics for Obj1 to Obj4. Values are normalized with respect to the maximum value of each characteristic. It shows that for optimized temperature rise, the weight becomes the highest. For optimized weight, the cost also will be near the least. Temperature rise becomes the highest when cost is optimized. And for optimized efficiency, all other characteristics will be in the middle. The result trends for inner and outer rotor PMSGs are close to each other although there are differences in values. For better understanding in Figure 11, efficiency has been replaced with total loss since we will minimize all the objective functions.

Figure 12 shows the change of 4 optimization variables over the iterations when the Obj5 is used as the objective function. It can be seen that airgap length and PM angle converge to their lower and higher limits, respectively.

The trend of change in 4 output characteristics is shown in Figure 13 for the Obj5 objective function. As shown, the cost increases over the initial low values as there is a conflict between different objectives that are combined in Obj5.

Figure 14 compares the optimized designs of inner and outer PMSGs and the 4 output characteristics using the Obj5 function. It can be seen that the optimized inner rotor PMSG has slightly higher weight and cost, slightly lower loss but considerably lower temperature rise. This is due to the higher heat dissipation surface of the outer stator.

The parameters of optimized inner and outer rotor PMSGs are presented in Table 6. The optimal value of PM width to pole pitch and slot per pole per phase is 0.8 and 10, respectively, which are their maximum values. The optimal values of the airgap flux and airgap length also tend to their lower bounds. Different limits of these optimization variables will be set if there are no other restrictions.

To show the effectiveness of the design optimization, optimized inner and outer rotor PMSGs are compared to another design optimization [11, 21] that included inner and outer as well as a double-stator single-rotor 5-MW PMSGs. As is evident from Figure 15, this article's design optimization has resulted in a considerable decrease in weight and material cost and an excellent increase in power density.

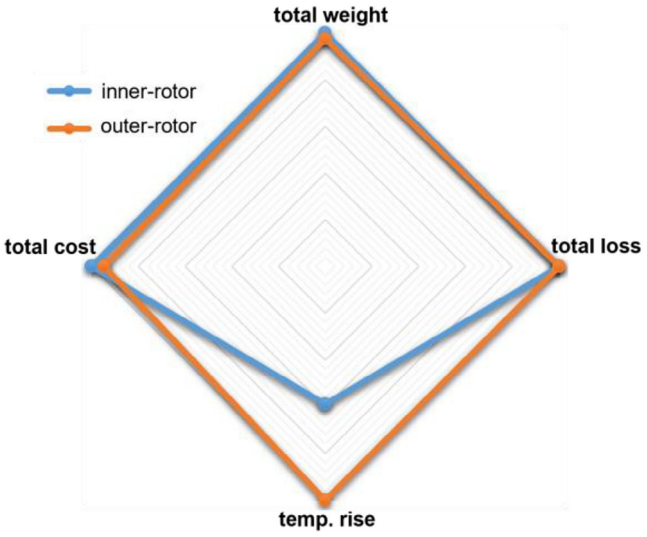

FIGURE 14 Comparison of Obj5 for inner and outer rotor PMSGs.

TABLE 6 Base and optimized PMSG parameters.

Parameter	Base PMSG	Optimized inner rotor PMSG	Optimized outer rotor PMSG
α	0.8	0.8	0.8
q_1	5	10	10
B_1(T)	0.8	0.7	0.7
J(A/m^2)	4e6	4000009	4000010
J_1(A/m)	33e3	49896	49961
g(mm)	15	10	10
r_g(mm)	500	468.8	501.7
L(m)	1.88	1.62	1.42
r_{outer}(mm)	637	579	605
N_{pb}	40	56	60
R_s(ohm)	0.0335	0.0416	0.0417
l_m(mm)	37.5	17.4	17.4
l_y(mm)	92	75.4	80.5
w_s(mm)	14	7.2	7.8
l_s(mm)	22.5	30.2	30.2
L_s(mH)	4.2	12.6	13.4
Total weight (kg)	11365	7783	7567
Efficiency (%)	98.5	98.6	98.6
Total cost (k$)	138450	57288	54118
temperature rise (°C)	133	98.6	167.8

The purpose of this comparison is to demonstrate the advantages of the presented analytical model, selected optimization parameters, and the optimization method in this article when it comes to designing PMSGs. According to these comparisons, the PMSGs designed in our article demonstrate significant improvement in design indexes.

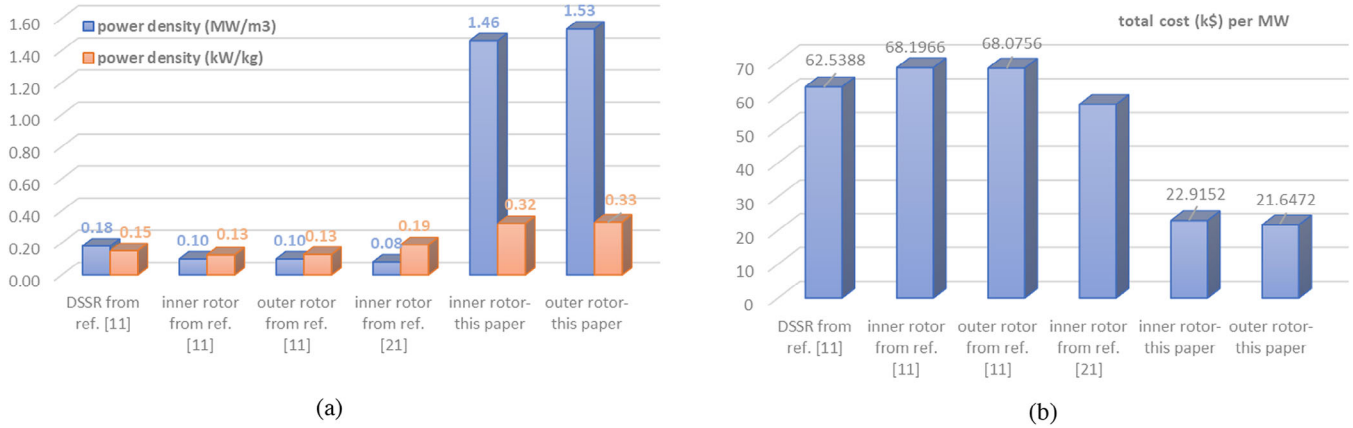

FIGURE 15 Comparison of machine indexes. (a) Power density and (b) total material cost per MW.

6 | CONCLUSIONS

By considering two topologies of radial flux structure, the PMSG parameters were optimized to achieve optimal performance for wind energy applications. As a first step, an analytical model was developed and a numerical simulation was conducted to verify it. Although the analytical model does not account for some 3D effects in electromagnetic characteristics, the comparison of numerical and analytical results indicates that it is sufficiently accurate for use in the optimization algorithm. Since there were some conflicting parameters and design constraints, GA was used to find the best designs for the desired objectives. In the process of optimization, different designs were generated, each of which was tailored to meet the specific performance requirements. Based on the comparison of the optimized designs of this article with those of another study, it is evident that there has been a significant improvement in both power density and material costs.

AUTHOR CONTRIBUTIONS

Reza Yazdanpanah: Conceptualization; formal analysis; methodology; software; validation; visualization; writing—original draft; writing—review and editing. **Seyed Abolfazl Mortazavizadeh**: Conceptualization; formal analysis; methodology; software; validation; visualization; writing—original draft; writing—review and editing. **Mohammad Salehian**: Data curation; software; visualization. **David Campos-Gaona**: Funding acquisition; resources; supervision; writing—review and editing. **Olimpo Anaya-Lara**: Funding acquisition; resources; supervision; writing—review and editing.

ACKNOWLEDGEMENTS

This project has received funding from the European Union's Horizon 2020 Research and Innovation Programme under Grant Agreement No. 101007135.

CONFLICT OF INTEREST STATEMENT

The authors certify that they have no affiliations with or involvement in any organization or entity with any financial interest, or non-financial interest in the subject matter or materials discussed in this manuscript.

DATA AVAILABILITY STATEMENT

The data that support the findings of this study are available from the corresponding author upon reasonable request.

ORCID

Reza Yazdanpanah https://orcid.org/0000-0003-2528-3062

REFERENCES

1. O'Connell, R., Phadke, A., O'Boyle, M., Clack, C.T., Denholm, P., Ernst, B.: Carbon-free energy: How much, how soon? IEEE Power Energy Mag. 19(6), 67–76 (2021)
2. European Commission: An EU strategy to harness the potential of offshore renewable energy for a climate neutral future (2020). https://eur-lex.europa.eu/legal-content/EN/TXT/HTML/?uri=CELEX%3A52020DC0741
3. Reulein, D., Tiwari, S., Hestvik, B., Kvannli, A., Pinel, D., Andresen, C.A., et al. (eds.): Large-scale offshore wind development and decarbonization pathways of the Norwegian energy system. In: 2023 19th International Conference on the European Energy Market (EEM). IEEE, Piscataway (2023)
4. Swibki, T., Salem, I.B., Amraoui, L.E., (eds.): Modeling and control of direct-drive PMSG-based offshore wind turbine under rigorous wind conditions. In: 2020 6th IEEE International Energy Conference (ENERGYCon). IEEE, Piscataway (2020)
5. Dinh, V.N., Nguyen, H.X., (eds.): Design of an Offshore Wind Farm Layout. In: Proceedings of the 1st Vietnam Symposium on Advances in Offshore Engineering. Springer, Singapore (2019)
6. Fu, J., Yan, X., Wang, D., Liu, H., Cheng, D., (eds.): L/HVRT scheme of offshore permanent magnet synchronous wind turbine. 18th International Conference on AC and DC Power Transmission (ACDC 2022). IET, Stevenage (2022)
7. Flannigan, C., Carroll, J., Leithead, W., (eds.): Operations expenditure modelling of the X-Rotor offshore wind turbine concept. J. Phys.: Conf. Ser. 2265, 032054 (2022)
8. Leithead, W., Camciuc, A., Amiri, A.K., Carroll, J., (eds.): The X-Rotor offshore wind turbine concept. J. Phys.: Conf. Ser. 1356, 012031 (2019)
9. Bjerkebæk, A.: Design sensitivity analysis of the Xrotor offshore wind turbine jacket structure. Master thesis, NTNU (2023)
10. Ha, Y., Meshgin Kelk, H.: A unique optimized double-stator permanent-magnet synchronous generator in high-power wind plants. Energy 143, 973–9 (2018)

11. Gul, W., Gao, Q., Lenwari, W.: Optimal design of a 5-MW double-stator single-rotor PMSG for offshore direct drive wind turbines. IEEE Trans. Ind. Appl. 56(1), 216–25 (2020)
12. Mamur, H., Şahin, C., Karaçor, M., Bhuiyan, M.R.A.: Design and fabrication of an outer rotor permanent magnet synchronous generator with fractional winding for micro-wind turbines. IET Electr. Power Appl. 14(12), 2273–82 (2020)
13. Sethuraman, L., Maness, M., Dykes, K., (eds.): Optimized generator designs for the DTU 10-MW offshore wind turbine using GeneratorSE. In: 35th Wind Energy Symposium. National Renewable Energy Laboratory (NREL), Golden, CO (2017)
14. Yazdanpanah, R., Mirsalim, M.: Hybrid electromagnetic brakes: design and performance evaluation. IEEE Trans. Energy Convers. 30(1), 60–9 (2015)
15. Li, H., Chen, Z., Polinder, H.: Optimization of multibrid permanent-magnet wind generator systems. IEEE Trans. Energy Convers. 24(1), 82–92 (2009)
16. Boldea, I., Tutelea, L.N.: Electric Machines: Transients, Control Principles, Finite Element Analysis, and Optimal Design with MATLAB®. CRC Press, Boca Raton, FL (2021)
17. Polinder, H., FFAvd, P., GJd, V., Tavner, P.J.: Comparison of direct-drive and geared generator concepts for wind turbines. IEEE Trans. Energy Convers. 21(3), 725–33 (2006)
18. Mirjalili, S.: Evolutionary algorithms and neural networks. In: Studies in Computational Intelligence, vol. 780. Springer, Cham (2019)
19. Spall, J.C.: An overview of the simultaneous perturbation method for efficient optimization. Johns Hopkins APL Tech. Dig. 19(4), 482–92 (1998)
20. Salehian, M., Sefat, M.H., Muradov, K.: A robust, multi-solution framework for well placement and control optimization. Comput. Geosci. 26(4), 897–914 (2022)
21. Tutelea, L., Torac, I., Isfanuti, A.S., Popa, A., Boldea, I., (eds.): 10MW, 10 rpm, 30 Hz spoke Ferrite and bonded NdFeB-rotor wind PMSG preliminary design with FEM validations for 6 rotor variants. In: 2021 International Aegean Conference on Electrical Machines and Power Electronics (ACEMP) & 2021 International Conference on Optimization of Electrical and Electronic Equipment (OPTIM). IEEE, Piscataway (2021)

How to cite this article: Yazdanpanah, R., Mortazavizadeh, S.A., Salehian, M., Campos-Gaona, D., Anaya-Lara, O.: Design optimization of inner and outer-rotor PMSGs for X-ROTOR wind turbines. IET Renew. Power Gener. 18, 2605–2618 (2024). https://doi.org/10.1049/rpg2.13111